Theory of a Zeeman Laser. II*

M. SARGENT III† AND WILLIS E. LAMB, JR.
Yale University, New Haven, Connecticut
AND
R. L. FORK
Bell Telephone Laboratories, Murray Hill, New Jersey

(Received 4 May 1967)

The general theory of a Zeeman laser given in part I is used to analyze laser operation in axial and transverse magnetic fields. The analysis is illustrated by graphs of intensities and beat frequencies versus cavity detuning and magnetic field strength. Among the topics discussed are frequency-locking effects due to cavity anisotropy, the dependence of competition between polarization modes on magnetic field strength for various atomic angular momenta, and the measurement of atomic decay rates and g values using a laser in a magnetic field.

I. INTRODUCTION

In paper I,[1] a theory of a laser subject to a uniform dc magnetic field at any angle to the maser axis was given in extension of a non-Zeeman treatment by Lamb.[2] The theory resulted in amplitude- and frequency-determining equations for multimode operation of the laser with possibly anisotropic cavity loss and resonance and an active medium consisting of atoms which may have arbitrary angular momenta, isotopic abundance, and hyperfine structure. Computer programs were described which can be used to analyze these equations in their fullest generality, yielding among other things graphs of intensities and frequencies of oscillation versus time, cavity detuning and anisotropy, magnetic field strength, or any other laser parameter.

In this paper, we give and illustrate graphically some simple examples of that theory. In general it is convenient to discuss the results for zero magnetic field operation before discussing those for nonzero magnetic field operation. This approach should make the theory useful to those interested in the zero-field limit alone. Steady-state solutions of the equations are found either algebraically or by integrating the differential equations. The latter method is sometimes preferred when more than one steady state is stable and is required in the analysis of time-varying configurations typically created by cavity anisotropy. The competition between polarization modes can be expressed in terms of a "coupling" parameter C. This depends markedly on the atomic angular momenta but decreases sharply as a function of magnetic fields in all cases. A graphical representation of these relationships is given in Secs. III and VI.

Marked variations of the optical-field intensity with magnetic field and cavity tuning appear in the theoretical curves. These can be related to the satisfaction of certain resonance conditions, such as the matching of the Zeeman splitting to the resonator mode spacing. These resonances lend themselves naturally to the measurement of atomic parameters, for example level widths and g values; however, careful consideration must be given to complicating factors of laser operation such as Q anisotropies and population differences between magnetic sublevels. The handling of the complex influence of these factors is included to demonstrate the versatility of the theory.

II. AXIAL MAGNETIC FIELD IN ± BASIS

Although the basis $\boldsymbol{\epsilon}_\pm$ given by[3] (I.18) is somewhat more complicated than the x-y basis (I.17) for off-axis magnetic fields, it is particularly suited to the axial magnetic field case for which the laser z axis $\mathbf{k}$ coincides with the atomic z axis $\mathbf{k}'$. Then $\mathbf{j}=\mathbf{j}'$ as well (see Fig. 1, paper I), and transitions for which $a'=b'\pm1$ contribute to $E_\pm$. In fact from (I.34), one has "direction cosines"

$$f_{\pm1}(\pm)=\sqrt{2}, \qquad f_{\pm1}(\mp)=f_0(\pm)=0. \tag{1}$$

The amplitude- and frequency-determining equations are (I.81) and (I.82) with (I.83) and

$$\boldsymbol{\alpha}_{n\pm\,\pm}=-\tfrac{1}{2}i\nu g_{n\pm\,\pm}+\nu(\epsilon_0\hbar K)^{-1}$$
$$\times\sum_j (a_j/u_j)\sum_{a'}\sum_{b'}\delta_{a',b'\pm1}(\wp_{a'b'})^2$$
$$\times\bar{N}_{a'b'}Z[\gamma_{a'b'}+i(\omega_{a'b'}-\nu_{n\pm})], \tag{2}$$

$$\boldsymbol{\alpha}_{n\pm\,\mp}=-\tfrac{1}{2}i\nu g_{n\pm\,\mp}. \tag{3}$$

References to equation numbers defining the variables in (2) and (3) are given following (I.83).

* The work of two of the authors (M. Sargent III and W. E. Lamb, Jr.) was supported in part by the National Aeronautics and Space Administration, in part by the General Physics Division, Air Force Office of Scientific Research, and for M. Sargent, in part by Bell Telephone Laboratories. The main results of the paper were given at the American Physical Society meeting, Mexico City, August, 1966. See M. Sargent III, Bull. Am. Phys. Soc. **11**, 714 (1966).

This paper is based in part on material submitted by M. Sargent III in partial fulfillment of the requirements for the degree of Doctor of Philosophy at Yale University.

† Present address: Bell Telephone Laboratories, Inc., Holmdel, New Jersey.

[1] M. Sargent III, W. E. Lamb, Jr., and R. L. Fork, preceding paper, Phys. Rev. **164**, 436 (1967); referred to as Paper I.

[2] W. E. Lamb, Jr., Phys. Rev. **134**, A1429 (1964).

[3] A reference (I.10) refers to Eq. (10) of Paper I.

Furthermore, no terms occur in these equations with nonzero third-order relative phase angles except when they would occur in the scalar theory (3 or more oscillating spatial modes). To see this, we note that the δ functions in (I.83) require that

$$q-r+s=\pm 1. \tag{4}$$

From (1) only terms with $q, r, s=\pm 1$ contribute to the polarization. Hence (4) implies

$$r=q \quad \text{or} \quad r=s. \tag{5}$$

By definition [see Eq. (I.33)], q, r, and s are the changes in magnetic quantum numbers corresponding to $E_{\mu'}$, $E_{\rho'}$ and $E_{\sigma'}$, respectively. Thus, because of (1) and (5), the polarization of $E_{\rho'}$ must equal that of $E_{\mu'}$ or that of $E_{\sigma'}$. Our assertion follows by definition of the relative phase angle (I.72). In particular there are no terms with nonzero, slowly varying relative phase angles in one or two spatial mode oscillation for this field orientation.

III. SINGLE-MODE OPERATION, AXIAL FIELD

For single-mode operation, the electric field (I.7) may be written

$$\mathbf{E}(z,t)=\tfrac{1}{2}\{E_+\boldsymbol{\varepsilon}_+\exp[-i(\nu_+t+\varphi_+)] +E_-\boldsymbol{\varepsilon}_-\exp[-i(\nu_-t+\varphi_-)]\}U(z)+\text{c.c.}, \tag{6}$$

where $\boldsymbol{\varepsilon}_\pm$ are given by (I.18). Using the relative phase angle

$$\psi=(\nu_+-\nu_-)t+(\varphi_+-\varphi_-), \tag{7}$$

this becomes

$$\mathbf{E}(z,t)=\tfrac{1}{2}\sqrt{2}\{(E_++E_-)\cos(\nu_+t+\varphi_+-\tfrac{1}{2}\psi)[\mathbf{i}\cos(\tfrac{1}{2}\psi) -\mathbf{j}\sin(\tfrac{1}{2}\psi)]+(E_+-E_-)\sin(\nu_+t+\varphi_+-\tfrac{1}{2}\psi) \times[-\mathbf{i}\sin(\tfrac{1}{2}\psi)-\mathbf{j}\cos(\tfrac{1}{2}\psi)]\}U(z). \tag{8}$$

In the course of time the vector $\mathbf{E}(z,t)$ (for fixed z) describes an ellipse with major axis $|(E_++E_-)U(z)|/\sqrt{2}$ and minor axis $|(E_+-E_-)U(z)|/\sqrt{2}$. The principal axes are rotated an angle $\frac{1}{2}\psi$ from the x and y axes. Thus, in general, the electric field describes an ellipse rotating counterclockwise with angular velocity $\frac{1}{2}\dot{\psi}$, where from (7)

$$\dot{\psi}=(\nu_+-\nu_-)+(\dot{\varphi}_+-\dot{\varphi}_-). \tag{9}$$

The beat frequency $\Delta\nu$ is

$$\Delta\nu=\left[\int_0^{2\pi}\dot{\psi}^{-1}d\psi\right]^{-1}. \tag{10}$$

If $\dot{\psi}$ is constant, $\Delta\nu=(\dot{\psi}/2\pi)$.

The mode indices μ, ρ, σ, and n are all equal and the sums in (I.83) reduce to sums over the polarizations alone. We now assume the anisotropy matrix G_n (I.10) is diagonal in the $\pm$ representation. The resulting amplitude- and frequency-determining equations have the same form as those for two-mode operation in the scalar theory.[4] Writing them explicitly in the $\alpha, \beta, \theta, \sigma, \rho$, and τ notation and taking $\gamma_{a'a''}=\gamma_a$, $\gamma_{b'b''}=\gamma_b$, $\gamma_{a'b'}=\gamma_{ab}$, $N_{a'b'(n-n')}\delta_{a',b'\pm 1}=\bar{N}$ for all a', b', a'', b'', and the δ-function approximation (I.79), one has

$$\dot{E}_\pm=E_\pm(\alpha_\pm-\beta_\pm E_\pm^2-\theta_{\pm\mp}E_\mp^2), \tag{11}$$

$$\nu_\pm+\dot{\varphi}_\pm=\Omega_\pm+\sigma_\pm+\rho_\pm E_\pm^2+\tau_{\pm\mp}E_\mp^2, \tag{12}$$

where

$$\alpha_\pm=\Gamma\sum_j(a_j/u_j)\sum_{a'}\sum_{b'}\delta_{a',b'\pm 1}(\wp_{a'b'})^2Z_i[\gamma_{ab}+i(\omega_{a'b'}-\nu_\pm)]-\nu/2Q_\pm, \tag{13}$$

$$\beta_\pm=(\Gamma'/\gamma_a\gamma_b)\sum_j(a_j/u_j)\sum_{a'}\sum_{b'}\delta_{a',b'\pm 1}(\wp_{a'b'})^4[1+\gamma_{ab}^2\mathfrak{L}(\omega_{a'b'}-\nu_\pm)], \tag{14}$$

$$\theta_{\pm\mp}=\tfrac{1}{2}\Gamma'\sum_j(a_j/u_j)\sum_{a'}\sum_{b'}\delta_{a',b'\pm 1}(\wp_{a'b'})^2(\wp_{a'\mp 2,b'})^2\{(\gamma_b\gamma_{ab})^{-1}[\gamma_{ab}^2\mathfrak{L}(\omega_{a'b'}-(\pm\delta_a)-\nu_\pm)+\gamma_{ab}^2\mathfrak{L}(\delta_{\cdot})] +\mathfrak{L}_a(2\delta_a)[(\gamma_a\gamma_{ab}-2\delta_a^2)\mathfrak{L}(\delta_a)+[\gamma_a\gamma_{ab}-(\pm 2\delta_a)(\omega_{a'b'}-\nu_\pm)]\mathfrak{L}(\omega_{a'b'}-\nu_\pm)]\} +\text{same with } (\gamma_a\leftrightarrow\gamma_b,\ \delta_a\rightarrow\delta_b \text{ and } \wp_{x'\mp 2,b'}\rightarrow\wp_{a',b'\pm 2}). \tag{15}$$

$$(1/Q_\pm)=\text{Re}(g_{\pm\pm}), \tag{16}$$

$$\Omega_\pm=\Omega+\tfrac{1}{2}\nu\,\text{Im}(g_{\pm\pm}), \tag{17}$$

$$\sigma_\pm=\Gamma\sum_j(a_j/u_j)\sum_{a'}\sum_{b'}\delta_{a',b'\pm 1}(\wp_{a'b'})^2Z_r[\gamma_{ab}+i(\omega_{a'b'}-\nu_\pm)], \tag{18}$$

$$\rho_\pm=-(\Gamma'/\gamma_a\gamma_b)\sum_j(a_j/u_j)\sum_{a'}\sum_{b'}\delta_{a',b'\pm 1}(\wp_{a'b'})^4\gamma_{ab}(\omega_{a'b'}-\nu_\pm)\mathfrak{L}(\omega_{a'b'}-\nu_\pm), \tag{19}$$

[4] Reference 2, pp. A1441–1442.

$$\tau_{\pm\mp}=-\tfrac{1}{2}\Gamma'\sum_j(a_j/u_j)\sum_{a'}\sum_{b'}\delta_{a',b'\pm1}(\wp_{a'b'})^2(\wp_{a'\mp2,b'})^2\{(\gamma_b\gamma_{ab})^{-1}[(\pm\delta_a)\gamma_{ab}\mathfrak{L}(\delta_a)$$
$$+\gamma_{ab}(\omega_{a'b'}-(\pm\delta_a)-\nu_\pm)\mathfrak{L}(\omega_{a'b'}-(\pm\delta_a)-\nu_\pm)]+\mathfrak{L}_a(2\delta_a)[(\pm\delta_a)(2\gamma_{ab}+\gamma_a)\mathfrak{L}(\delta_a)$$
$$+[(\pm\delta_a)2\gamma_{ab}+\gamma_a(\omega_{a'b'}-\nu_\pm)]\mathfrak{L}(\omega_{a'b'}-\nu_\pm)]\}+\text{same with }(\gamma_a\leftrightarrow\gamma_b,\ \delta_a\rightarrow\delta_b,\text{ and }\wp_{a'\mp2,b'}\rightarrow\wp_{a',b'\pm2}),\quad(20)$$

$$\nu=\tfrac{1}{2}(\nu_++\nu_-),\quad(21)$$

$$\Gamma=\nu\bar{N}(\epsilon_0\hbar K)^{-1},\qquad\Gamma'=\tfrac{1}{4}\pi^{1/2}\hbar^{-2}\Gamma,\quad(22)$$

$$\mathfrak{L}_\alpha(\Delta\omega)=[\gamma_\alpha^2+(\Delta\omega)^2]^{-1},\qquad\alpha=a,b,$$

$$\mathfrak{L}(\Delta\omega)=[\gamma_{ab}^2+(\Delta\omega)^2]^{-1},\quad(23)$$

$$\omega_{a'b'}=\omega_0+(\mu_B/\hbar)H(g_aa'-g_bb'),\quad(24)$$

$$\delta_\alpha=(\mu_B/\hbar)Hg_\alpha+\tfrac{1}{2}(\nu_--\nu_+),\quad(25)$$

where ω_0 is the zero magnetic field frequency of the jth isotope at its line center. Here for typographical simplicity we have suppressed the subscript j on the ω's and g's. In writing (24) and (25) we have assumed the magnetic field splitting is a linear function of field strength.

In terms of the relative excitation $\mathfrak{N}$ defined by (I.67), the Γ of (22) is replaced by

$$\Gamma=\tfrac{1}{2}\nu\,\mathrm{Re}(g_{\mathbf{hh}})\mathfrak{N}\left[\sum_j(a_j/u_j)\sum_{k=-1}^{1}|f_k(p_h)|^2\sum_{a'}\sum_{b'}\delta_{a',b'\pm k}(\wp_{a'b'})^2Z_i[\gamma_{ab}+i(\omega_0-\nu_{\mathbf{h}t})]\right]^{-1}.\quad(26)$$

Here $\nu_{\mathbf{h}t}$ is chosen so that the expression in brackets is a maximum and the subscript **h** indicates the mode with polarization p_h which oscillates at threshold.

The conditions for steady-state oscillation are

$$\dot{E}_\pm=0.\quad(27)$$

The stable steady-state solutions are as given[4] in the scalar two-mode theory. If $\alpha_+\leq0$ and $\alpha_-\leq0$, $E_+=E_-=0$. If $\alpha_\pm<0$ and $\alpha_\mp>0$, the intensity

$$I_\pm=E_\pm^2\quad(28)$$

equals 0 and $I_\mp=\alpha_\mp/\beta_\mp$. If both α's>0 and the effective α,

$$\alpha_\pm'=\alpha_\pm-\theta_{\pm\,\mp}(\alpha_\mp/\beta_\mp),\quad(29)$$

is less than 0, $I_\pm=0$ and $I_\mp=\alpha_\mp/\beta_\mp$. If α_+', $\alpha_-'>0$, the behavior depends on the value of the "coupling" parameter

$$C=\theta_{+\,-}\theta_{-\,+}/\beta_+\beta_-.\quad(30)$$

If $0\leq C<1$ (weak coupling), both polarizations oscillate with the intensities

$$I_\pm=(\alpha_\pm\beta_\mp-\theta_{\pm\,\mp}\alpha_\mp)/(\beta_+\beta_--\theta_{+\,-}\theta_{-\,+}).\quad(31)$$

If $C>1$ (strong coupling), either polarization oscillates alone (which depends on past history) with the intensity

$$I_\pm=\alpha_\pm/\beta_\pm.\quad(32)$$

If $C=1$ (neutral coupling), any solution satisfying

$$\alpha_+=\beta_+I_++\theta_{+\,-}I_-\quad(33)$$

may be stable.

Having determined E_+ and E_-, one may use (12) to find $\nu_++\dot{\varphi}_+$ and $\nu_-+\dot{\varphi}_-$. The electric field as given by (8) is then completely determined apart from phase factors. The steady-state calculation may be iterated in a self-consistent fashion by using in Eqs. (13)–(26) the values of $\nu_\pm+\dot{\varphi}_\pm$ given by (12). Computer analysis has shown that this process converges almost invariably in two steps to sufficient accuracy.

In zero field (14) and (15) become

$$\beta_\pm=2(\Gamma'/\gamma_a\gamma_b)\sum_j(a_j/u_j)[1+\gamma_{ab}^2\mathfrak{L}(\omega_0-\nu_\pm)]$$
$$\times\sum_{a'}\sum_{b'}\delta_{a',b'\pm1}(\wp_{a'b'})^4,\quad(34)$$

$$\theta_{\pm\,\mp}=2(\Gamma'/\gamma_a\gamma_b)\sum_j(a_j/u_j)[1+\gamma_{ab}^2\mathfrak{L}(\omega_0-\nu_\pm)]$$
$$\times\sum_{a'}\sum_{b'}\delta_{a',b'\pm1}(\wp_{a'b'})^2\{(\wp_{a'\mp2,b'})^2+(\wp_{a',b'\pm2})^2\},\quad(35)$$

so that the magnitude of C is determined totally by the relative size of the sum of matrix elements for $\beta_\pm$ and that for $\theta_{\pm\,\mp}$. Heer and Graft[5] gave a table of the ratio of these sums $[=\sqrt{C}$ by combining (30), (34), and (35)$]$ for a number of common transitions. For $J=1\leftrightarrow J=1$ or $0\leftrightarrow1$, $C=1$, i.e., neutral coupling. For $1\leftrightarrow2$, $C=(22/46)^2=0.228$, i.e., weak coupling, but for $2\leftrightarrow2$, $C=(42/26)^2=2.6$, which gives strong coupling. In general they found that transitions for which $J_a=J_b\pm1$ were weak coupled and those for which $J_a=J_b$ were strong coupled except for the special cases $0\leftrightarrow1$, $1\leftrightarrow1$, which were neutral coupled. Similar conclusions concerning stability were given by Polder and Van Haeringen,[6] who derived a zero-field expression for $\epsilon^{-1}\dot{\epsilon}$, where the eccentricity $\epsilon=(E_+-E_-)/(E_++E_-)$. Neither group mentioned $\frac{1}{2}\leftrightarrow\frac{1}{2}$,

[5] C. V. Heer and R. D. Graft, Phys. Rev. **140**, A1088 (1965).
[6] D. Polder and W. Van Haeringen, Phys. Letters **19**, 380 (1965); W. Van Haeringen, *ibid.* **24A**, 65 (1967); Phys. Rev. **158**, 256 (1967).

which has no coupling at all (the θ terms are identically zero). Any observed coupling must be due to effects neglected in our analysis, such as pressure or radiative decay[7] from level a to b.

To the extent that $(\mu_B/\hbar)H(g_a-g_b)$ can be neglected, one can see by comparing (14) and (34) that the effect of a magnetic field on the β's is to introduce a frequency translation equal to the field splitting. The height of the peak is not changed. Comparing (15) and (35), however, one sees that in the θ's a magnetic field not only introduces a displacement but also decreases the height of the peak, for the factor of 1 in (35) is replaced in (15) by dimensionless Lorentzians of the field splitting. These Lorentzians result from the fact that as the Zeeman splitting is increased two waves of

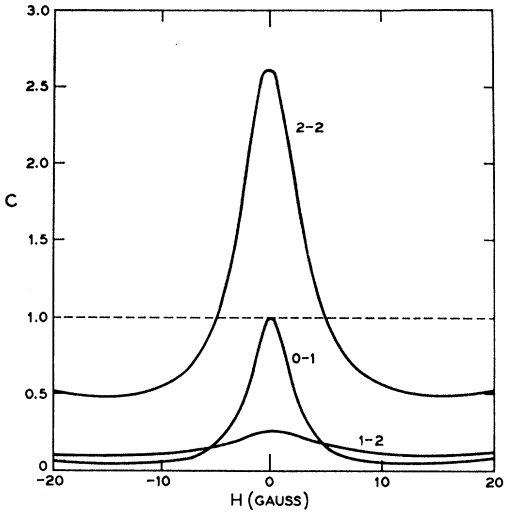

FIG. 1. The coupling parameter C given by (30) is plotted versus axial magnetic field in gauss under central tuning for (in order of decreasing coupling) $J=2\leftrightarrow J=2$, $0\leftrightarrow1$, $1\leftrightarrow2$. The other laser parameters are $\gamma_a=18$ MHz, $\gamma_b=40$ MHz, $\gamma_{ab}=29$ MHz, $Ku=1010.0$ MHz, $\mathfrak{N}_\pm=1.20$, $g_a=g_b=1.295$; there is only one isotope, no nuclear spin, $\Omega_+=\Omega_-$ and $Q_+=Q_-$. The dashed line for $C=1$ represents neutral coupling and divides the graph into a strong-coupling region ($C>1$) and a weak-coupling region ($C<1$).

opposite polarization travelling in the same direction cease to interact with atoms in the same velocity range. The result is that the coupling decreases in a somewhat Lorentzian fashion as the magnetic field is increased. This is illustrated in Fig. 1, where the coupling parameter C is plotted versus magnetic field for central tuning and a number of J values. Note that the transition $2\leftrightarrow2$ goes out of the strong-coupling region for a field of about 5 G.

Figures 2–4 show graphs of the actual intensities versus cavity detuning for the transitions $0\leftrightarrow1$, $1\leftrightarrow2$ and $2\leftrightarrow2$, respectively. For the $0\leftrightarrow1$ transition (Fig. 2) there are two regions placed symmetrically about line

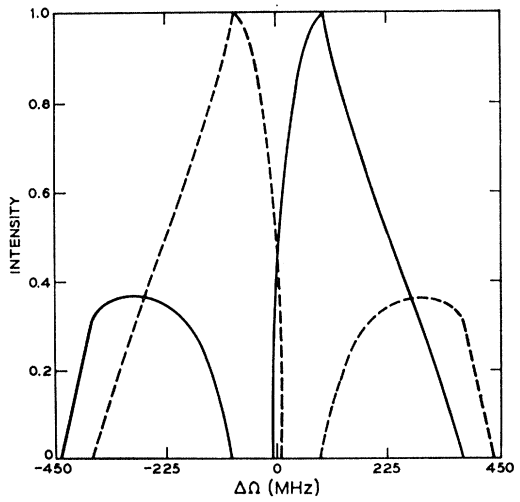

FIG. 2. Intensities I_+ (dashed line), I_- (solid line) versus cavity detuning in MHz for a $0\leftrightarrow1$ transition, and axial field of 1 G and other parameters the same as in Fig. 1. The intensities are given in arbitrary units.

center in which one polarization "inhibits" the other. In these regions the effective α for one mode is negative, and it cannot oscillate. This dependence on detuning was given earlier by Fork and Sargent[8,9] and some discussion of this case has been given by Culshaw and Kannelaud.[10] Experimentally, this transition (He-Ne, 1.52μ) is strong-coupled for fields of less than 1.5 G, probably because of pressure effects neglected in our

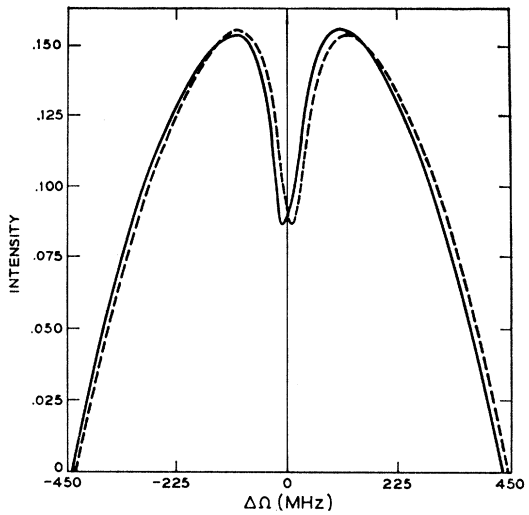

FIG. 3. Intensities I_+, I_- versus cavity detuning in MHz for a $1\leftrightarrow2$ transition, a field of 1 G and other parameters the same as in Fig. 2.

[7] M. I. D'Yakonov and V. E. Perel, Opt. i Spektroskopiya **20**, 472 (1966) [English transl.: Opt. Spectry. (USSR) **20**, 257 (1966)].

[8] R. L. Fork and M. Sargent III, Phys. Rev. **139**, A617 (1965).

[9] R. L. Fork and M. Sargent III, in *Physics of Quantum Electronics*, edited by P. L. Kelley, B. Lax, and P. E. Tannenwald (McGraw-Hill Book Company, Inc., New York, 1966), pp. 611–619.

[10] W. Culshaw and J. Kannelaud, Phys. Rev. **145**, 257 (1966).

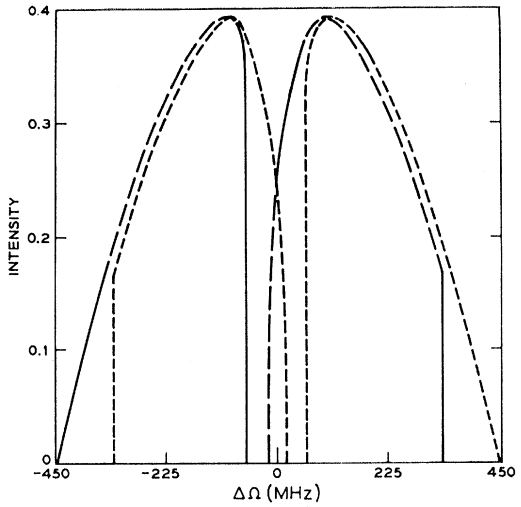

FIG. 4. Intensities I_+, I_- versus cavity detuning in MHz for a $2\leftrightarrow 2$ transition, an axial field of 5 G and other parameters as in Fig. 2. The long dashes are for I_- and indicate strong coupling, i.e., only one polarization may oscillate with the intensity given by (32).

analysis.[11–13] The $1\leftrightarrow 2$ transition (Fig. 3) shows relatively little coupling between the modes and the central-tuning dip characteristic of a Brewster window laser appears in both polarizations. For 1 G, the $2\leftrightarrow 2$ transition is strong-coupled over the entire detuning range. The intensity of the polarization mode which happens to oscillate exhibits a dip similar to the output of the zero-field Brewster window laser, but at a detuning equal to the field splitting. Increasing the field to 5 G reduces the coupling greatly in all three transitions, and Fig. 4 shows how the $2\leftrightarrow 2$ laser is bistable only in the certain regions (bistability is indicated by use of a dashed line for I_- instead of a solid line as in Figs. 2 and 3).

Figure 5 shows a graph of the intensities versus magnetic field for a $0\leftrightarrow 1$ transition and central tuning. The magnetic field tuning dip in the intensities can be significantly different from the conventional central tuning dip.[14] This can be understood by noting that with central tuning and an axially symmetric cavity, one may drop the $\pm$ subscripts on α, β, and θ so that

$$I_+=I_-\equiv I=(\alpha/\beta)[1-(\theta/\beta)]/[1-(\theta/\beta)^2]$$
$$=(\alpha/\beta)/[1+\sqrt{C}]. \quad (36)$$

The factor α/β exhibits a dip similar to that met in the zero-field Brewster window laser,[14] the principal difference being that the standing wave saturation is reduced by magnetically shifting the gain curves relative to the mode frequency rather than by detuning the cavity. The factor $(1+\sqrt{C})^{-1}$ dips because C has a maximum for zero magnetic field as explained above. It is interesting to note that while the dip in α/β results from the nonlinear interaction of atoms within a given velocity range with waves having the same polarization and traveling in opposite directions (a standing wave dip), the dip in $(1+\sqrt{C})^{-1}$ results from waves having orthogonal polarizations and traveling in the same direction (traveling wave dip).

In (14) and (15) the standing wave terms are those having arguments of the form $(\omega_{a'b'}-\nu_\pm)$, that is, those terms containing Lorentzian functions with arguments that depend on the relative position of an atomic resonance and the oscillation frequency. The traveling wave terms contain Lorentzians having the arguments δ_a or δ_b, i.e., they are independent of the relative positions of the atomic resonance and the oscillation frequency, but do show a dependence on the magnetic field splitting and possibly on the frequency difference between two oscillating modes. These dips may be resolved and used in the measurement of atomic constants (see Sec. VIII).

Combining (9), (10), and (12) one has the beat frequency

$$2\pi\Delta\nu=\dot{\psi}=\Omega_+-\Omega_-+\sigma_+-\sigma_-+\rho_+E_+^2-\rho_-E_-^2$$
$$+\tau_{+-}E_-^2-\tau_{-+}E_+^2. \quad (37)$$

For small signal oscillation and $\Omega_+=\Omega_-$ this is given by the difference $\sigma_+-\sigma_-$, which increases approximately linearly with magnetic field. For higher levels of excitation, the third-order differences $\rho_+E_+^2-\rho_-E_-^2$ and $\tau_{+-}E_-^2-\tau_{-+}E_+^2$ may in low magnetic fields be of larger magnitude and opposite sign and push the beat frequency negative as shown in Fig. 6. Such a de-

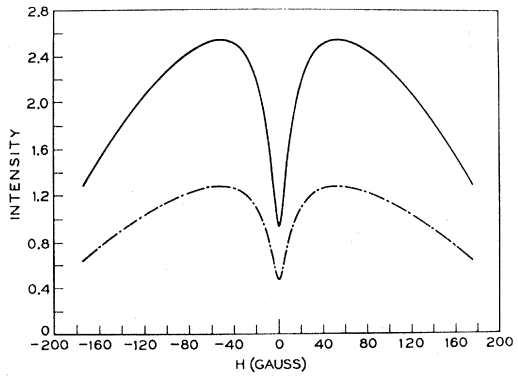

FIG. 5. Mode intensities versus axial magnetic field for zero detuning and operation on a single resonator mode. The solid line represents total intensity and the dash-dot curve the equal intensities of the + and − polarizations as given by Eq. (36). We have chosen parameters $J_a=1$, $J_b=0$, $g_a=1.295$, $\mathfrak{N}_\pm=1.20$, $\gamma_a=18.0$ MHz, $\gamma_b=40.0$ MHz, $\gamma_{ab}=29.0$ MHz, and $Ku=1010.0$ MHz. In this figure, Figs. 15–20, 22, and 23, the intensities are given in arbitrary units equal to 1.64 times those in Figs. 2–4, 7, 8, 13, and 14.

[11] R. L. Fork and W. J. Tomlinson, IEEE J. Quantum Electron. **QE-2**, 23 (1966).
[12] W. J. Tomlinson and R. L. Fork, following paper, Phys. Rev. **164**, 466 (1967).
[13] H. deLang and G. Bouwhis, Phys. Letters **20**, 383 (1966); H. deLang, thesis, State University of Utrecht, 1966, especially pp. 57–75 (unpublished).
[14] Reference 2, p. A1438.

pendence was observed first by Culshaw and Kannelaud[15] (without, however, noting the change in sign of $\dot{\psi}$) and was discussed theoretically for $J=0\leftrightarrow J=1$ by Fork and Sargent,[8] Rozanov and Tulub,[16] Culshaw and Kannelaud,[10] and for any J values by D'Yakonov.[17]

From (19) and (20), one sees that in zero field, the ratio of τ to $\rho=\sqrt{C}$ and consequently $\dot{\psi}$ will depend on the angular-momentum values J_a and J_b. In particular if other parameters are held constant, the minimum in beat frequency is much deeper for a $0\leftrightarrow 1$ transition where the τ's are larger than the ρ's than for a $1\leftrightarrow 2$ transition.

IV. OPERATION INVOLVING TWO SPATIAL MODES—AXIAL MAGNETIC FIELD

There are no terms involving relative phase angles in the third-order amplitude- and frequency-determining equations for the oscillation on two spatial modes (see Sec. II). Assuming the anisotropy matrix G_n, (I.10) is diagonal in the $\pm$ representation and using (28), the laser equations (I.81) and (I.82) reduce to

$$\dot{I}_n=2I_n[\alpha_n-\sum_m \theta_{nm}I_m], \tag{38}$$

$$\nu_n+\dot{\varphi}_n=\Omega_n+\sigma_n+\sum_m \tau_{nm}I_m, \tag{39}$$

where $\mathbf{n}$ and $\mathbf{m}$ each index the two polarizations for the spatial modes n and m, respectively, and thus have the explicit values $1-$, $1+$, $2-$ and $2+$. The coefficients α_n, θ_{nm}, σ_n, and τ_{nm} are given in the approximations of Sec. III by (13), (14), (18), and (19), respectively, with the subscript $\pm$ replaced by $\mathbf{n}$ or equivalently $n\pm$. The θ_{nm} and τ_{nm} coupling orthogonal polarizations are given by (15) and (20), respectively, with the subscript $\pm$ replaced by $\mathbf{n}$, $\mp$ by $\mathbf{m}$ and for $n\neq m$ with the factor $N_2/\bar{N}$ [see (I.59) for definition of N_2] multiplying $\mathfrak{L}(\omega_{a'b'}-\nu_n)$. The θ_{nm} and τ_{nm} coupling different spatial modes ($n\neq m$) but identical polarizations are given by (15) and (20) as above with the additional replacements of $\pm\delta_a$ and $\pm\delta_b$ by $\frac{1}{2}(\nu_m-\nu_n)$, and $\wp_{a'\mp 2,b'}$ and $\wp_{a',b'\pm 2}$ by $\wp_{a'b'}$.

The steady-state conditions are

$$\dot{I}_n=0. \tag{40}$$

Since there are four intensities here any of which may or may not be oscillating, there are $2^4=16$ solutions. Those having negative values of I_n are nonphysical and must be discarded. Using (14), (15) and the remarks following (39), one sees that ordinarily

$$\theta_{nm}\geq 0 \tag{41}$$

for all $\mathbf{n}$ and $\mathbf{m}$. It follows from this and (38) that intensities corresponding to negative α's equal zero.

For a given solution, the subscript $\mathbf{n}$ takes on values contained in two sets, the set indexing nonzero intensities $\mathfrak{N}$ and that indexing zero intensities $\mathfrak{Z}$. In this terminology, the sixteen solutions to (40) are of the form

$$\begin{aligned} &I_n=0, && \mathbf{n}\in\mathfrak{Z},\\ &I_n=\sum_m (\theta^{-1})_{nm}\alpha_m, && \mathbf{n},\mathbf{m}\in\mathfrak{N}, \end{aligned} \tag{42}$$

where θ^{-1} is the inverse of the truncated θ matrix whose indices belong to $\mathfrak{N}$.

We investigate now the stability of the steady-state solutions which are physical, i.e., $I_n\geq 0$ for all $\mathbf{n}$. For this we write

$$I_n=I_n^{(s)}+\epsilon_n, \tag{43}$$

where ϵ_n is a small deviation from the steady-state intensity $I_n^{(s)}$ satisfying (42). Substituting (43) into (38), one has

$$\dot{\epsilon}_n=-2I_n^{(s)}\sum_m \theta_{nm}\epsilon_m+O(\epsilon^2) \tag{44}$$

for $\mathbf{n},\mathbf{m}\in\mathfrak{N}$ and

$$\dot{\epsilon}_n=2\epsilon_n[\alpha_n-\sum_m \theta_{nm}I_m^{(s)}]+O(\epsilon^2) \tag{45}$$

for $\mathbf{n}\in\mathfrak{Z}$, $\mathbf{m}\in\mathfrak{N}$. The condition for a stable steady state is

$$\epsilon_n\to 0,\ t\to\infty, \tag{46}$$

which is true if and only if the real parts of the eigenvalues of the matrix in (44) with elements $-I_n^{(s)}\theta_{nm}$ are negative and the effective α's:

$$\alpha_n'=\alpha_n-\sum_m \theta_{nm}I_m^{(s)},\ \mathbf{n}\in\mathfrak{Z},\mathbf{m}\in\mathfrak{N} \tag{47}$$

in (45) are negative.

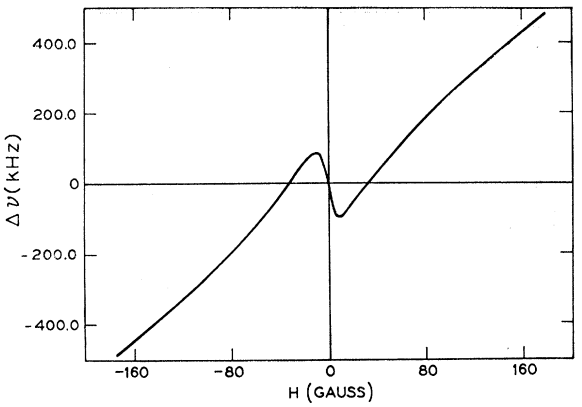

FIG. 6. Beat frequency $\Delta\nu$ in kHz given by (37) versus magnetic field. Same parameters as in Fig. 5.

[15] W. Culshaw and J. Kannelaud, Phys. Rev. **136**, A1209 (1964). See also P. T. Bolwijn, in *Physics of Quantum Electronics* edited by P. L. Kelley, B. Lax, and P. E. Tannenwald, (McGraw-Hill Book Company, Inc., New York, 1966), p. 620; thesis, State University of Utrecht, 1967, especially Chap. 5 (unpublished).

[16] N. N. Rozanov and A. V. Tulub, Dokl. Akad. Nauk SSSR, Ser. Fiz. **165**, 1280 (1965) [English transl.: Soviet Phys.—Doklady **10**, 1209 (1966)].

[17] M. I. D'Yakonov, Zh. Eksperim. i Teor. Fiz. **49**, 1169 (1965) [English transl.: Soviet Phys.—JETP **22**, 812 (1966)]. In the derivation of the coefficients D'Yakonov assumes that $\nu_+=\nu_-$. This assumption is not valid for our purposes since there may be appreciable circular birefringence.

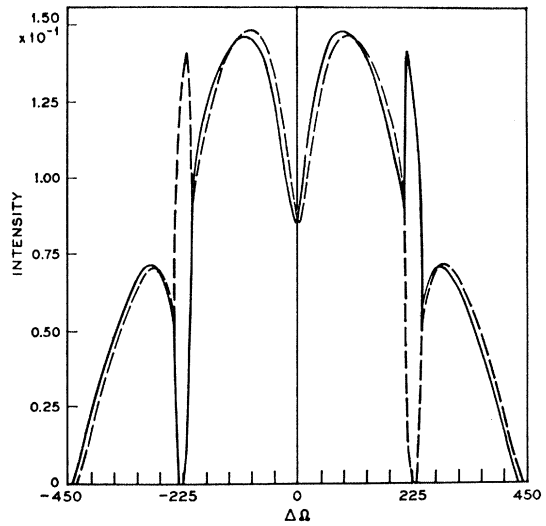

FIG. 7. Intensities I_+ (dashed curve) and I_- (solid curve) as functions of cavity detuning for two-spatial mode operation, a 1↔2 transition, an axial magnetic field of 1 G, a mode separation of 450 MHz ($\Omega_2=\Omega_1+450$ MHz) and other parameters the same as in Fig. 1. The intensities of the first cavity mode are given in the region of detuning -450 MHz$\leqq\Delta\Omega_1=\Omega_1-\omega\leqq 0$ and those for the second are given by moving 450 MHz above into the region $0\leqq\Delta\Omega_2=\Omega_2-\omega\leqq 450$ MHz.

The computer programs include a routine to try each of the 16 solutions given by (41) and test their stability using (44) and (45). Figure 7 gives graphs of the intensities I_+ and I_- for two adjacent longitudinal modes and a 1↔2 transition.

A steady state of some practical interest (see Sec. VIII) occurs for excitations too small for normal two spatial mode operation, but with a magnetic field splitting equal to the cavity mode spacing. The result is that one cavity mode oscillates with one polarization and the other mode with the orthogonal polarization.

V. EFFECT OF CAVITY ANISOTROPY

In a given representation cavity anisotropy is conveniently divided into two categories. The first consists of anisotropy which is represented by nonequal diagonal elements of the anisotropy matrix G_n (I.10) and the second of that represented by nonzero off-diagonal elements. In this section we illustrate the effects of both kinds using the ± representation and examples similar to those of Sec. III.

Cavity anisotropy of the first kind, e.g., $Q_+\neq Q_-$ or $\Omega_+\neq\Omega_-$, is included in the equations of Secs. III and IV. If $Q_+\neq Q_-$, one can see from (31) that curves of intensity versus cavity detuning become asymmetric and regions of mode inhibition (see Fig. 2) become narrower or cease to exist for the mode of higher Q and become larger for that of smaller Q. This is illustrated in Fig. 8, where a graph of intensities versus cavity detuning is given for the same parameters as in Fig. 2 except that $Q_+=1.001Q_-$. Nonequal cavity resonances ($\Omega_+\neq\Omega_-$) affect the intensities in a fashion similar to an axial magnetic field H provided

$$H=\tfrac{1}{2}(\hbar/\mu_B g_a)(\Omega_+-\Omega_-). \tag{48}$$

In fact, if $g_a=g_b$ and $\bar{N}_+=\bar{N}_-$, the coefficients in the amplitude and frequency-determining equations (11) and (12) are the same for a circular birefringence $\Omega_+-\Omega_-$ as for a field given by (48). The beat frequency (37), however, is approximately $\Omega_+-\Omega_-$, whereas it is much smaller in the equivalent magnetic field (48).

Cavity anisotropy of the second kind leads to terms with phase factors $\exp\pm i\psi$ in the equations [see (7), (I.81), and (I.82)]. As we shall see presently, these terms may cause frequency locking,[18] i.e., $\nu_+=\nu_-$ and ψ assumes a definite value. We now analyze this second variety of anisotropy in terms of the important special case for which the off-diagonal elements of the anisotropy matrix result from an x-y Q anisotropy.[19]

Treating the effect of an axial magnetic field in the ± basis, one has from (I.10) and (I.20) the off-diagonal elements of G_n:

$$g_{+-}=g_{-+}=\tfrac{1}{2}(Q_x^{-1}-Q_y^{-1}). \tag{49}$$

Adding the corresponding anisotropy terms to (11) and (12) as indicated by (I.81) and (I.82), one has

$$\dot{E}_\pm=E_\pm(\alpha_\pm-\beta_\pm E_\pm^2-\theta_\pm\mp E_\mp^2)$$
$$-\tfrac{1}{4}[(\nu/Q_x)-(\nu/Q_y)]E_\mp\cos\psi, \tag{50}$$

$$\nu_\pm+\dot{\varphi}_\pm=\Omega_\pm+\sigma_\pm+\rho_\pm E_\pm^2+\tau_\pm\mp E_\mp^2$$
$$\pm\tfrac{1}{4}(E_\pm/E_\mp)\sin\psi[(\nu/Q_x)-(\nu/Q_y)], \tag{51}$$

where the coefficients are given by (13) through (26) with

$$Q_\mp^{-1}=\tfrac{1}{2}(Q_x^{-1}+Q_y^{-1}), \tag{52}$$

and the relative phase angle ψ is given by (7). Using

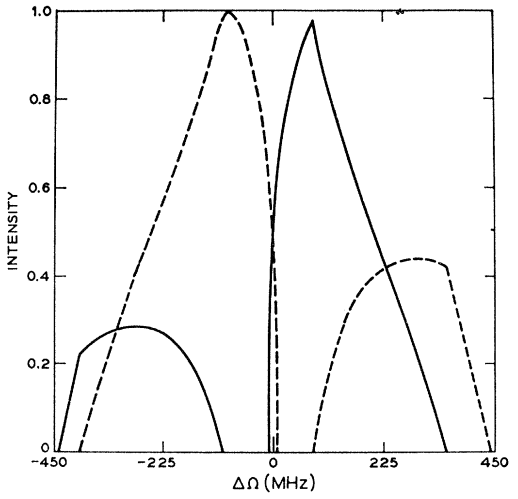

FIG. 8. Intensities I_+, I_- versus cavity detuning in MHz for same parameters as in Fig. 2, except $Q_+=1.001Q_-$.

[18] Reference 2, pp. A1444-5.

[19] M. Sargent III, W. E. Lamb, Jr., W. J. Tomlinson, and R. L. Fork, Bull. Am. Phys. Soc. **12**, 90 (1967).

(9) and (50) one has

$$\dot{\psi}=\Omega_+-\Omega_-+\sigma_+-\sigma_-+\rho_+E_+^2-\rho_-E_-^2+\tau_+{}_-E_-^2$$
$$-\tau_-{}_+E_+^2+\tfrac{1}{4}[(\nu/Q_x)-(\nu/Q_y)]$$
$$\times[(E_+/E_-)+(E_-/E_+)]\sin\psi. \quad (53)$$

Some insight into (50) and (53) can be gained by considering an x-y Q anisotropy sufficiently small that the term with $\cos\psi$ in (50) may be neglected. Equations (50) are then decoupled from (53) and may be solved using the steady-state theory of Sec. III. In this approximation, (53) has the form

$$\dot{\psi}=a+b\sin\psi, \quad (54)$$

where a and b are constants for a given set of laser parameters. This has the implicit solution

$$t(\psi)=\int_{\psi_0}^{\psi} dx(a+b\sin x)^{-1}, \quad (55)$$

where ψ_0 is the value of ψ at $t=0$. For $|a/b|>1$, ψ changes monotonically in time and $t(\psi)$ has the value

$$t(\psi)=2(a^2-b^2)^{-1/2}\{\tan^{-1}[(b+a\tan\tfrac{1}{2}\psi)(a^2-b^2)^{-1/2}]$$
$$-\tan^{-1}[(b+a\tan\tfrac{1}{2}\psi_0)(a^2-b^2)^{-1/2}]\}. \quad (56)$$

When $\psi=\psi_0\pm 2\pi$, the expression $\{\cdots\}$ equals $\pm\pi$ and the beat frequency (10) is

$$\Delta\nu=[t(\psi_0\pm 2\pi)]^{-1}=\pm(2\pi)^{-1}(a^2-b^2)^{1/2}, \quad (57)$$

where the sign is that of the coefficient a. If $|a/b|\leq 1$,

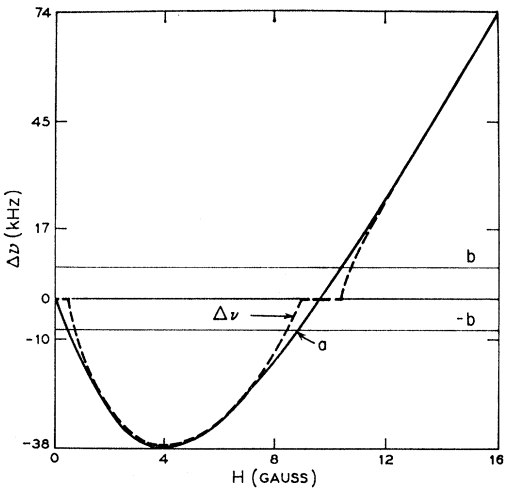

FIG. 9. Plots of the coefficients a (curved solid line) and b (horizontal solid lines) of (54) and the beat frequency $\Delta\nu$ (curved dashed line) of (57) versus magnetic field in gauss. The frequencies of circularly polarized modes are locked together for fields with $|a/b|\leqq 1$, and the phase angle ψ is given by ψ_2 of (58). The x-y Q anisotropy $\frac{1}{4}\nu(Q_x^{-1}-Q_y^{-1})=0.004$ MHz. Other laser parameters are $\gamma_a=15$ MHz, $\gamma_b=35$ MHz, $\gamma_{ab}=25$ MHz, $Ku=420.6$ MHz, $\mathfrak{N}_\pm=1.10$, $\Omega_+=\Omega_-$, $Q_+=Q_-$; there is only one isotope, and no nuclear spin.

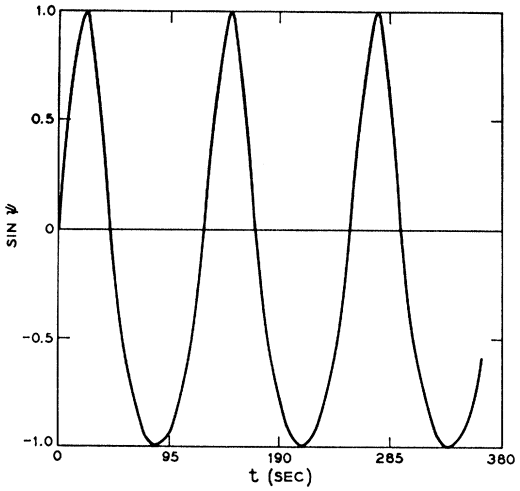

FIG. 10. Time plot of $\sin\psi$ obtained from an integration of (53) using an axial field of 7.5 G. The other parameters are the same as in Fig. 9.

the integral (55) diverges, i.e., $t\to\infty$ as

$$\psi\to\psi_1=-\sin^{-1}(a/b)$$

or

$$\psi\to\psi_2=\pi+\sin^{-1}(a/b). \quad (58)$$

Thus ψ approaches one of these values asymptotically in time. As explained in the discussion following (8), the electric field vector describes in the course of time an ellipse whose principle axes are rotated by an angle $\frac{1}{2}\psi$ from the x and y axes.

To illustrate the decoupled limit, let us now describe the results of a time integration of (53) in which the magnetic field was slowly increased from zero and the intensities I_+ and I_- were obtained using the steady-state theory of Sec. III. The parameters used were similar to those of Fig. 6, with the addition of the small x-y Q anisotropy $\frac{1}{4}[(\nu/Q_x)-(\nu/Q_y)]=0.004$ MHz. Because the cavity was centrally tuned ($\Omega_+=\Omega_-=\omega_0$), the intensity I_+ was equal to I_- and had the magnetic field dependence given in Fig. 5. Therefore the coefficient b of (54) was a constant with the value 0.008 MHz. In the decoupled approximation, the magnetic field dependence of the coefficient a of (54) is similar to that of $\Delta\nu$ in Fig. 6. Thus, as the field is increased from 0, the magnitude of a becomes larger than that of b, then smaller and finally larger. This is shown in Fig. 9, where the curved solid line is a graph of a versus magnetic field and the horizontal solid lines are graphs of b. The dashed line is a graph of the resultant beat frequency (57). Here we see $\Delta\nu=0$ for $|a/b|\leq 1$, i.e., frequency locking has taken place. At 7.6 G $|a/b|>1$ and $\dot{\psi}$ fluctuates as a function of ψ between -25 kHz for $\sin\psi=-1$ and -12 kHz for $\sin\psi=+1$. Accordingly ψ spends most of the time near, 90° as is illustrated by the graphs of $\sin\psi$ versus time in Fig. 10.

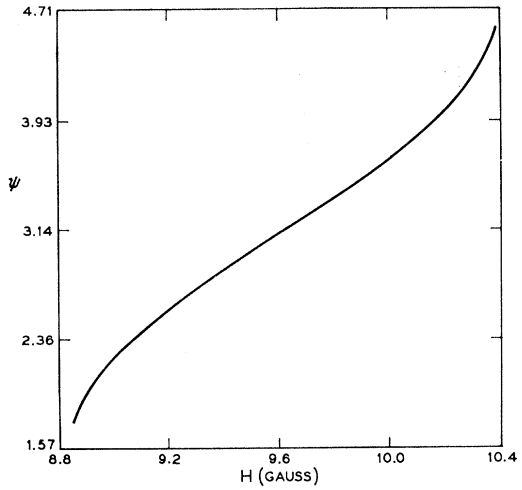

FIG. 11. Plot of ψ versus magnetic field in gauss as given by (58b) in the second locked region of Fig. 9.

Near $H=0$ or in the vicinity of $H=10$ G, $a\cong b$ and only the asymptotic solution ψ_2 of (58) is stable[20] as is easily shown by a small vibrations analysis. The magnetic field dependence of ψ in the second locking region of Fig. 9 is shown in Fig. 11.

An integration[21] of the coupled equations (50) and (53) was made for the parameters above as the magnetic field was increased from 7.5 to 10.0 G. The time dependence of $\dot{\psi}$ and ψ was almost identical to that given by the decoupled approximation above and the intensities were amplitude modulated characteristically less than 2% at the beat frequency $\Delta\nu$. Thus one is justified in interpreting these results in terms of the decoupled approximation.

There are cases, however, for which a and b in (54) are appreciably time-dependent and the decoupled approximation breaks down. Tomlinson and Fork[12] have given examples of this kind for which the ratio $|a/b|$ oscillated around unity causing $\dot{\psi}$ and ψ in turn to oscillate nonsinusoidally. This is not a locked state, for $\dot{\psi}$ does not remain equal to zero for any length of time.

Tomlinson and Fork[12] have achieved rather remarkable quantitative agreement between the theory given here and experiments on the 1.52-μ ($0\leftrightarrow1$) and 0.6328-μ ($1\leftrightarrow2$) transitions in the He-Ne laser. The reader is referred to their paper for further discussion.

A magnetic field dependence of $\Delta\nu$ similar to that given in Fig. 9 was observed by Kannelaud and Culshaw,[22] who accounted[23] for the zero-field locking region by an x-y Q anisotropy. Their treatment is an extension of the scalar theory[2] in which they used a $\frac{1}{2}\leftrightarrow\frac{1}{2}$ transition and assumed the locked state. As we have seen in Sec. III, the use of the $\frac{1}{2}\leftrightarrow\frac{1}{2}$ transition with no third-order coupling terms, i.e., $C=0$ should (see Fig. 1) approximate to some degree the weakly coupled $1\leftrightarrow2$ transition, but a quantitative agreement with experiment is precluded. D'Yakanov[17] gave a weak-field theory valid for central tuning and arbitrary angular momenta which deals with the zero-field locking region in the presence of an x-y Q anisotropy and regions of higher fields without this anisotropy. Pelikan[24] came closest to our approach in his explicit consideration of phase angles and derived amplitude- and frequency-determining equations for the $0\leftrightarrow1$ transition. Velzel[25] has given the form of these equations and indicated how to include cavity anisotropy of a more general nature. Doyle and White[26] gave a zero-field analysis for atoms with arbitrary angular momenta which includes cavity anisotropy of the first kind (diagonal elements of G), but in general not of the second kind (off-diagonal elements).

VI. TRANSVERSE MAGNETIC FIELD IN x-y REPRESENTATION

The x-y representation is particularly suited to the transverse magnetic field case, for magnetic quantum number changes of ±1 correspond to E_{nx} and those of 0 to E_{ny}. This results because E_{ny} and E_{nx} are the components parallel and perpendicular to the magnetic field, respectively (see Fig. 1, Paper I). In fact, from (I.34), one has the direction cosines

$$f_{\pm1}(x)=f_0(y)=1, \qquad f_{\pm1}(y)=f_0(x)=0. \tag{59}$$

The amplitude- and frequency-determining equations are (I.81) and (I.82) with (I.83), (59), and

$$\alpha_{nxx}=-\tfrac{1}{2}i\nu g_{nxx}+\tfrac{1}{2}\nu(\epsilon_0\hbar K)^{-1} \times\sum_{a'}(a_j/u_j)\sum_{a'}\sum_{b'}\delta_{a',b'\pm1}(\wp_{a'b'})^2 \times\bar{N}_{a'b'}Z[\gamma_{a'b'}+i(\omega_{a'b'}-\nu_{nx})], \tag{60}$$

$$\alpha_{nyy}=-\tfrac{1}{2}i\nu g_{nyy}+\tfrac{1}{2}\nu(\epsilon_0\hbar K)^{-1} \times\sum_{j}(a_j/u_j)\sum_{a'}\sum_{b'}\delta_{a',b'}(\wp_{a'b'})^2 \times\bar{N}_{a'b'}Z[\gamma_{a'b'}+i(\omega_{a'b'}-\nu_{ny})], \tag{61}$$

$$\alpha_{nxy}=-\tfrac{1}{2}i\nu g_{nxy},\ \alpha_{nyx}=-\tfrac{1}{2}i\nu g_{nyx}. \tag{62}$$

The problem is more complicated than that of the axial field in the $\pm$ basis for unless J_a or $J_b=0$, there are third-order terms with phase angles in (I.81) and (I.82). This may be understood in the following

[20] W. J. Tomlinson (private communication), to whom the authors are very grateful for numerous helpful discussions.
[21] The results were presented in the form of a computer movie of the standing wave electric field at the August, 1966, meeting of the American Physical Society. See M. Sargent III, Bull. Am. Phys. Soc. **11**, 714 (1966).
[22] J. Kannelaud and W. Culshaw, Phys. Rev. **141**, 237 (1966).
[23] W. Culshaw and J. Kannelaud, Phys. Rev. **141**, 228 (1966).
[24] H. Pelikan, Phys. Letters **21**, 652 (1966). Note that according to this work, phase locking cannot take place for $I_+=I_-$; Z. Physik **201**, 523 (1967).
[25] C. H. F. Velzel, Phys. Letters **23**, 72 (1966).
[26] W. M. Doyle and M. B. White, Phys. Rev. **147**, 359 (1966); Phys. Rev. Letters **17**, 467 (1966).

analysis along the lines of that given in Sec. II for the axial field.

If $J_a=1$ and $J_b=0$, then the magnetic quantum numbers b' and b'' defined in Fig. 2 of part I are zero. It follows from the definition of q, r and s [see Eq. (I.33) and (I.73)] that $r=q$ and $s=k$. In terms of the amplitudes, this implies that the polarization indices of $E_{\mu'}$ and $E_{\sigma'}$ must equal those of $E_{\rho'}$ and E_{n}, respectively. A similar argument holds for $J_a=0$, $J_b=1$. Thus, if either J_a or $J_b=0$, there are no third-order terms with slowly-varying phase angles for one or two spatial modes. If neither J_a nor J_b is zero, there are terms in (I.83) for which the magnetic quantum numbers $a'\neq a''$ or $b'\neq b''$. Consequently r does not have to equal q or s and the polarization index of $E_{\rho'}$ does not have to equal that of $E_{\mu'}$ or $E_{\sigma'}$. Even for single-spatial-mode operation, this allows slowly varying phase angle terms coupling the x and y fields for any electric-dipole transition except $0\leftrightarrow1$. This leads in general to a time-varying problem which may sometimes simplify in one of two possible limits: (1) If the phase angle terms are sufficiently rapidly oscillating, they tend to average to zero in time; (2) locking may take place, forcing the phase angle

$$\psi=(\nu_x-\nu_y)t+\varphi_x-\varphi_y \tag{63}$$

to a constant value, i.e., $\nu_x=\nu_y$. In either case, a steady-state solution may exist.

The latter case occurs for single-spatial-mode operation with central tuning ($\Omega_x=\Omega_y=\omega_0$) (single isotope) and equal populations of magnetic sublevels, for the coefficients in the frequency-determining equation are identically zero. This follows for ν_y because the coefficients are multiplied by vanishing frequency differences. It follows for ν_x because contributions to a coefficient for which $\Delta m=+1$ are equal in magnitude and opposite in sign to those for which $\Delta m=-1$. They add to zero in the sums over magnetic sublevels [see Eq. (I.83)]. A small amount of cavity anisotropy can force the phase angle ψ to a particular value as in the previous section [see Eq. (58)].

The phase factors $\exp i\psi_{\mathrm{n}\mu'\rho'\sigma'}$ in Eqs. (I.81) and I.82) all reduce either to unity or to $\exp\pm2i\psi$. For a given value of ψ, the third-order terms with $\exp\pm2i\psi$ may be combined with other terms having the same products $E_x^2E_y$ or $E_y^2E_x$. The combined coefficients depend on ψ and will be denoted by θ_{xy}' and θ_{yx}'. One may then discuss the interaction between polarizations along the lines given for the axial field in Sec. III by using the coupling parameter

$$C'=\theta_{xy}'\theta_{yx}'/\beta_x\beta_y. \tag{64}$$

Figure 12 gives C' versus magnetic field strength for central tuning, and a number of J values. Curves for values of $\psi=0$ and $\pi/2$ (linear and circular polarization) are given for the $1\leftrightarrow2$ and $2\leftrightarrow2$ transitions. Arguments similar to those for the axial field case

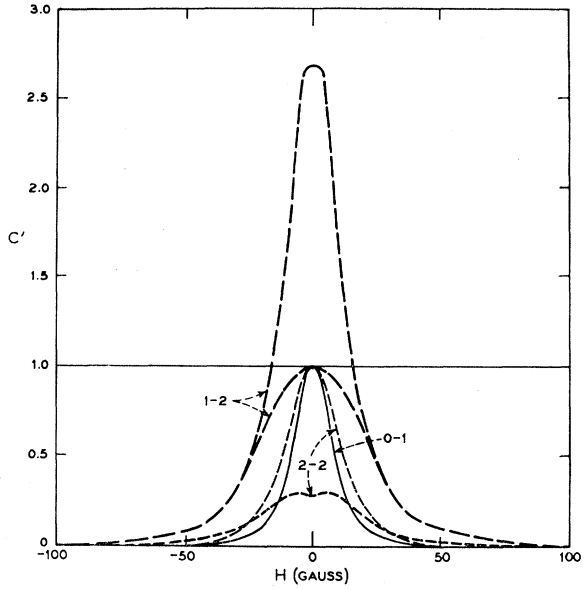

FIG. 12. Coupling parameter C' given by (64) versus transverse magnetic field in gauss for central tuning, $1\leftrightarrow2$, $0\leftrightarrow1$ and $2\leftrightarrow2$ transitions, $Q_x=Q_y$, $\Omega_x=\Omega_y$, and other parameters as in Fig. 1. The $0\leftrightarrow1$ curve is given by a solid line, the $1\leftrightarrow2$ curves by long dashes and the $2\leftrightarrow2$ by short dashes. The $1\leftrightarrow2$ curve with greater values in central tuning corresponds to ψ of (63) $=\pi/2$, that with smaller values to $\psi=0$. The reverse is true for the $2\leftrightarrow2$ curve.

show that in zero field C' is determined apart from ψ totally by the orbital angular momenta and that Lorentzians of the magnetic field splitting decrease the magnitudes of the θ's. Thus the coupling decreases with increasing magnetic fields. In noncentral tuning the phase factors $\exp(\pm2i\psi)$ will oscillate and modulate the amplitudes unless the cavity anisotropies are large enough to cause frequency locking. The effective value of C' will then also oscillate.

In Fig. 13 the intensities I_x and I_y at central tuning are graphed versus magnetic field for the $0\leftrightarrow1$, $1\leftrightarrow2$ and $2\leftrightarrow2$ transitions. As the field is increased from zero, the resonance frequencies of atoms contributing to I_x move away from the cavity resonance, at first causing I_x to increase and then decrease to 0. The resonance frequencies of atoms contributing to I_y are not shifted and I_y approaches a constant value. For field splittings equal to the cavity mode spacing, a special case of three-mode oscillation can occur, provided the losses for I_y are sufficiently greater than those for I_x. This is discussed in Sec. VIII using Fig. 21.

Figure 14 shows intensity curves versus detuning for $0\leftrightarrow1$ and $1\leftrightarrow2$ transitions in a field of 10 G. As indicated in Fig. 11, the coupling is considerably less than at zero field and I_y exhibits a central tuning dip. I_x is actually the sum of two terms with such dips whose centers are sufficiently displaced to give I_x a central peak. Amplitude modulation due to the phase terms has been suppressed in Fig. 14b since it did not appear in the experiments of Culshaw and Kannelaud.[10]

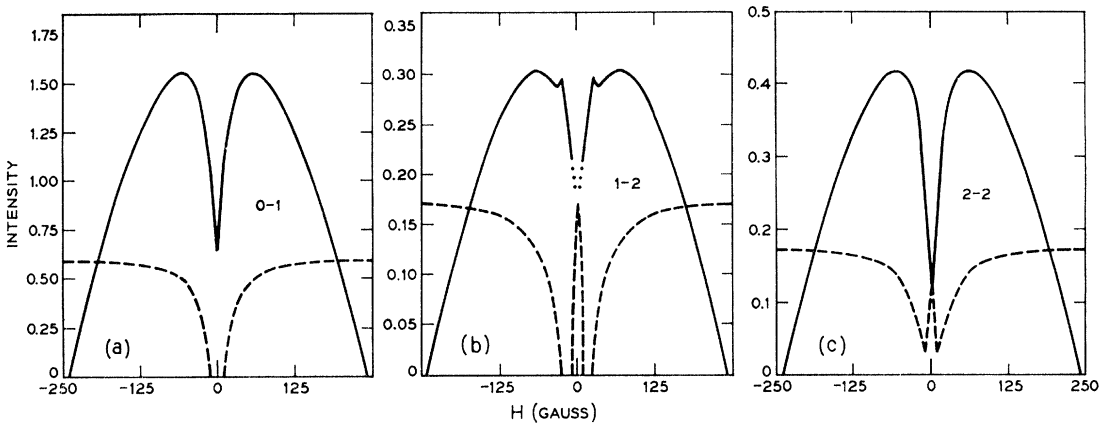

FIG. 13. Intensities I_x (solid line), I_y (dashed line) versus transverse magnetic field in gauss under central tuning for (a) $0\leftrightarrow1$, (b) $1\leftrightarrow2$ and (c) $2\leftrightarrow2$, respectively, and other parameters, as in Fig. 12.

Presumably this was due to the method of measurement in which the modulation was averaged out.

Culshaw and Kannelaud[10] gave equations for the $0\leftrightarrow1$ transition in a transverse magnetic field, neglecting anisotropy and making the approximations of Sec. III. They include graphs of the coefficients and intensities versus magnetic field. Durand[27] also gave equations for this transition, although his derivation depends upon a rate-equation approximation. D'Yakonov and Perel[7] have also considered this case, but without obtaining numerical results.

VII. ARBITRARILY ORIENTED FIELD

No major simplification occurs from choosing the x-y basis instead of the $\pm$ basis in the arbitrarily oriented field case except for central tuning where the beat frequency $2\pi\psi_{xy}$ can be zero for reasons given in Sec. VI. However, both bases are useful in studying the effects of misalignment of the magnetic field. For example, the x-y basis is used for estimating effects of a small axial component in the presence of a transverse field.

The magnitude of any term in the polarization is limited in part by the size of the products [see (I.63) and (I.83)] of the "direction cosines" $f_k(i)$ given by (I.34) and evaluated for the $\pm$ and x-y bases in Table I. Terms whose f products are zero for a perfectly aligned field in its favored basis [see (1) and (59)] have nonzero products for a misaligned field and may influence laser operation. The largest of these contain only one small f such as $1-\cos\Theta$ or $\sin\Theta$ in an approximately axial field or $\cos\Theta$ in a transverse. Thus for misalignment of 1° the largest additional terms are about 1.7% of the regular terms (only 0.03% for a $0\leftrightarrow1$ transition in axial field for which the largest term has a $\sin^2\Theta$). For the misalignments of 10% which occurred in the experiments of Culshaw and Kannelaud,[10] the largest additional terms may be as much as 10% of the regular terms. The behavior will be substantially different from that for a perfectly aligned field and should have locking regions due to the phase angles in the additional terms. Further discussion of misalignment is given in the next section.

VIII. MEASUREMENT OF ATOMIC DECAY RATES AND g VALUES

The determination of atomic decay rates (γ's) and g values for the laser atoms is necessary to a description of the laser operation. It is particularly convenient if these values can be determined from characteristics of the laser output since they are often unavailable or difficult to obtain by other methods. A measure of the level lifetimes is especially desirable since they are sensitive to the gas pressure in the laser and can vary significantly within the range of pressures conventionally used.

In this section we use the foregoing theory to determine the preferred conditions for measuring these various atomic parameters by means of the magnetic field tuned laser. Although the plots of mode intensity

TABLE I. The "direction cosines" of (I.34) evaluated for the $\pm$ basis (I.18) and the x-y basis (I.17).

$f_k(i)$	$i=+$	$-$	x	y
$k=+1$	$(1/\sqrt{2})(1+\cos\Theta)$	$(1/\sqrt{2})(1-\cos\Theta)$	1	$-i\cos\Theta$
-1	$(1/\sqrt{2})(1-\cos\Theta)$	$(1/\sqrt{2})(1+\cos\Theta)$	1	$i\cos\Theta$
0	$(i/\sqrt{2})\sin\Theta$	$-(i/\sqrt{2})\sin\Theta$	0	$\sin\Theta$

[27] G. Durand, IEEE J. Quantum Electron. **QE-2**, 448 (1966); Ann. Inst. Poincaré **A4**, 263 (1966).

versus magnetic field depend on all the atomic parameters it is often possible to choose the operating conditions so as to produce a distinct feature, such as a dip or switch in mode of maximum intensity, which depends principally on a single parameter. We will discuss conditions for producing these distinct features. Often it is possible to obtain the value of a parameter, such as one of the γ's, by a direct measurement of the experimental curve. In general, however, it would be necessary to carry out a least-squares fit of the data to the theoretical curves to obtain the γ values. For purposes of illustration we will give examples from the theory for a $J=0\leftrightarrow J=1$ transition (in which the a level is identified with the $J=1$ state) and also for a $J=1\leftrightarrow J=1$ transition.

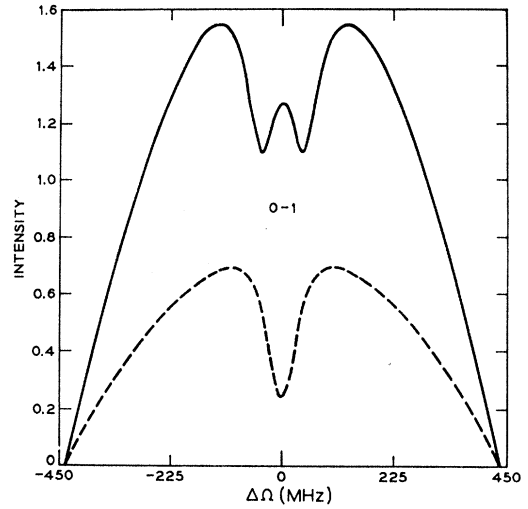

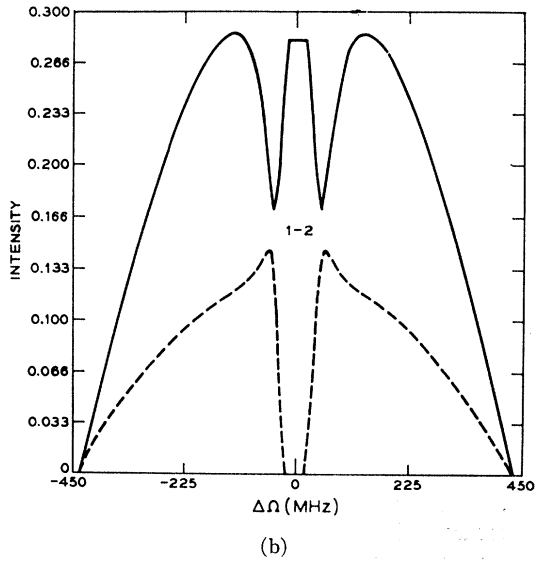

FIG. 14. Intensities I_x, I_y versus cavity detuning in MHz for transverse field of 20 G for (a) $0\leftrightarrow 1$ and (b) $1\leftrightarrow 2$ transitions, respectively, and other parameters as in Fig. 12. The phase angle terms occurring in the $1\leftrightarrow 2$ calculation have been averaged out.

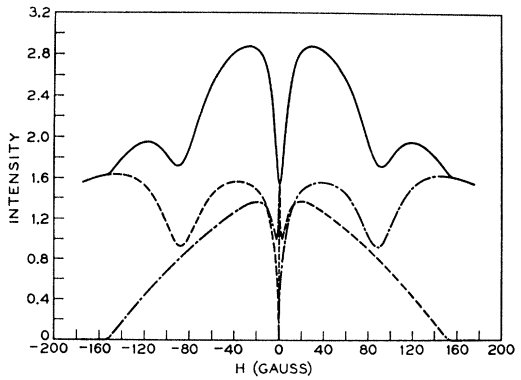

FIG. 15. Mode intensities versus axial magnetic field for 160 MHz detuning and operation on a single resonator mode. The traveling wave dip appears at $H=0$ and the standing wave dips occur for a value of H (± 88.25 G) at which the Zeeman splitting equals the laser detuning. In Figs. 15–20 the solid line represents total intensity, the dashed curve the plus polarization, and the dash-dot curve the minus polarization. Other parameters are the same as in Fig. 5.

The pertinent features of the variations in mode intensities as functions of applied magnetic field can be divided into two basic classes, those which occur because of a degeneracy of magnetic sublevels and those which occur for a splitting of magnetic sublevels which is equal to an integral multiple of the resonator mode spacing.[28] Both classes of variation permit lifetime measurements; however, the latter class also permits g-value measurements. The variations due to sublevel degeneracies will also permit g-value measurements in the special case where level crossings[29] occur for nonzero magnetic fields. Although these variations can be associated with the phenomena of depolarization of resonance radiation in the vicinity of magnetic sublevel degeneracies (Hanle effect), the distinct features of the variations depend on the nonlinear character of the interaction, in particular, the saturation of the velocity broadened gain curve and consequently are phenomena unique to the laser.

The variation in mode intensity occurring at a resonance generally appears as a "magnetic field tuning" dip (see Fig. 5) or reduction in the total intensity from the laser oscillator. As discussed in Sec. III this dip results partially from competition between waves traveling in opposite directions (standing wave contribution) and partially from competition between waves traveling in the same direction (traveling wave contribution). For an axial field these two contributions can be easily resolved by detuning the oscillator so that the resonator mode no longer coincides with the

[28] The resonance actually occurs when the Zeeman splitting equals the mode frequency difference $\nu_+-\nu_-$, which can differ from an integral multiple of the passive resonator mode spacing by several hundred kilocycles. This difference, caused by the dispersion of the medium, can amount to several parts in 1000 of the mode spacing and is not negligible in g-value determinations.

[29] F. Bitter, Appl. Optics 1, 1 (1962).

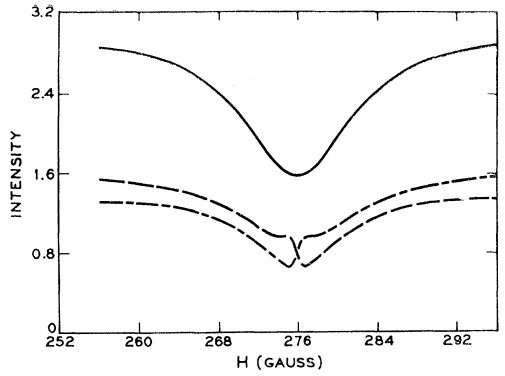

FIG. 16. Mode intensities versus axial magnetic field for 160 MHz detuning and operation on two resonator modes spaced by 1000 MHz. The features of the curve are similar to those in Fig. 15. The horizontal scale has been expanded to exhibit more clearly the crossover in mode intensities. Note also that the crossover occurs for a value of H (275.84 G) at which the Zeeman splitting equals the mode spacing. Other parameters are the same as in Fig. 5.

center of the gain curve. For example, given a $J=0\leftrightarrow J=1$ transition three dips appear as shown in Fig. 15. The first dip on the left in the total intensity curve is a standing wave dip caused by tuning the ω_- gain curve center through the cavity resonance. The second dip, which would be present even in the absence of standing waves, we will refer to as a traveling wave dip. It arises because the Zeeman splitting resolves the velocity classes with which oppositely polarized waves traveling in the same direction interact. The third dip, on the far right, is a standing wave dip caused by tuning of the ω_+ gain curve center through the cavity resonance. In this case we have assumed that oscillation occurs on only one mode of the resonator, and that this mode is located 160 MHz to the high-frequency side of the zero-field atomic resonance.

The resolution of these dips permits the extraction of the parameters γ_a and γ_{ab} separately since the principal terms describing the traveling wave portion of the dip are Lorentzians of width γ_a and the principal terms contributing to the standing wave portion of the dip are Lorentzians with width γ_{ab}. Provided $(\gamma_a+\gamma_b)/2=\gamma_{ab}$, as given in (I.46) and the initial detuning $\omega_0-\nu_0\gg\gamma_{ab}$, γ_a, the Lorentzians for the traveling wave part of the dip have a width γ_a. Even if γ_{ab} and γ_b are not known this feature permits a direct extraction of γ_a. Unfortunately $\gamma_{ab}\neq(\gamma_a+\gamma_b)/2$ except in very low pressure lasers.[30,31] However, this inequality can be plausibly incorporated in the present theory and useful measures of the γ's obtained by standard curve-fitting techniques.

An accuracy of 10% in measuring the dip width would provide a level lifetime value to an accuracy competitive with existing lifetime measurement methods.[32] An inspection of Fig. 15 shows that the standing wave dips in the individual intensity curves are more distinctive than the dips in the total intensity.

Consider the case where oscillation takes place on two modes of the resonator and only one polarization oscillates on each mode.[33] Resonances now occur for nonzero values of the magnetic field when the Zeeman splitting equals the mode frequency difference. For example, for a mode frequency difference Δ, similar curves to those shown in Figs. 5 and 15 are predicted, with the central dip now occurring at $H=\hbar\Delta/\mu_B g_a$. This, of course, provides a measurement of g_a. In this case, a trace similar to that in Fig. 5 is obtained if the modes are symmetrically positioned about the zero-field atomic resonance, and a trace similar to that in Fig. 15 is obtained if the center of the two resonator modes is shifted to the high-frequency side of the zero-field resonance by 160 MHz. The individual mode intensities exhibit a crossover in intensities at $H=\hbar\Delta/\mu_B g_a$. The crossover is less sharp and the excursions of the individual mode intensities are reduced from the single-mode case. These effects are caused by modifications in the N_2 and N_4 terms (I.59). Physically, this reflects a decrease in mode competition due to the spatial dependence of the mode phase relationships. The distribution of the active medium within the resonator also enters into these terms. The resulting curves are shown in Fig. 16, where the horizontal scale has been expanded to exhibit the crossover region more clearly. The crossover position is insensitive to resonator tuning and provides an attractive method for making a precise determination of g_a.

The precision of level lifetime and g-value measurements is affected by a number of phenomena not included in the simple theory of the Zeeman laser given in Sec. III. Collisions, population differences between magnetic sublevels, cavity anisotropies, or misalignment of the magnetic field (see Sec. VII) can shift the crossover or alter the dip making them less useful. All of these effects, except collisions, are handled by the general theory given above. Some of the features of collisions can be approximated by a simple model which treats γ_{ab} as a pressure-dependent parameter not equal to $(\gamma_a+\gamma_b)/2$, allows γ_a and γ_b to be pressure-dependent, and introduces a factor e^{ic} to represent a shift and asymmetry in the atomic interaction curve.[30] Using typical values for a collision broadened line[30] one obtains traces very similar to those already shown. Such a trace is shown in Fig. 17. The main alteration is a broadening of the mode intensity dips. The crossover in mode intensities at resonance again occurs at $H=\hbar\Delta/g_a\mu_B$; thus, in this approximation collisions would not impair the usefulness of the cross-

[30] R. L. Fork and M. A. Pollack, Phys. Rev. **139,** A1408 (1965). Collisions also cause the various multipole moments of the atomic states to relax at different rates, introducing additional complications. Some of these are briefly described in the following paper.

[31] A. Szöke and A. Javan, Phys. Rev. **145,** 137 (1966).

[32] W. R. Bennett, Jr., P. J. Kindlmann, and G. N. Mercer, Appl. Opt. Suppl. **2,** 34 (1965).

[33] Such a condition can be easily satisfied if the mode spacing and Zeeman splitting are comparable to or larger than the Doppler width of the gain curve. (See Sec. IV.)

over as a means of g-value measurement. The lack of dramatic change in the mode intensity curves is not surprising since the principal features arise from a competition between the two polarizations and marked changes are more to be expected from effects, such as population differences, which discriminate between the gain available to the two polarizations. The collision model described above does not so discriminate since it introduces identical shifts, broadenings, and asymmetries in both Zeeman split components of the gain curve.

Alterations in the predicted mode intensity curves caused by field misalignment are not dramatic until a certain angle of misalignment ($\sim$10°) is reached at which point the crossover disappears, and a marked asymmetry appears as shown in Fig. 18. A small misalignment (1°) produces a small shift ($\sim$0.04 G) of the value of magnetic field at which the mode crossover occurs. If unrecognized this could lead to an error of about one part in 7000 of the Zeeman splitting. It would seem that this source of error could usually be rendered negligible by exercising reasonable care in field alignment.

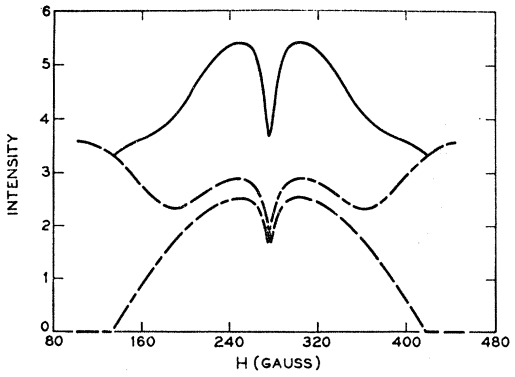

FIG. 17. Mode intensities versus axial magnetic field for 160 MHz detuning and oscillation on separate resonator modes. Collision effects have been introduced as described in the text. The parameters are the same as Fig. 5, except that now $\gamma_{ab}=80.0$ MHz, and c (the asymmetry parameter) $=0.03$.

In the case where both upper and lower atomic states have nonzero angular momenta it becomes possible to measure the g value and lifetimes for the two states a and b. The curve features rapidly become more complicated and the J values increase; however, for a $J=1\leftrightarrow J=1$ case the level characteristics appear in a simple way as shown in Fig. 19. The g values for the upper and lower states, $g_a=1.295$ and $g_b=0.999$, respectively, are sufficiently different to produce resolved magnetic tuning dips. The upper and lower level widths can be obtained from the two dip widths and the magnetic field values at which the dip minima occur provide a measure of the g values.

The precision of the g-values measurement appears to be most seriously affected by Q differences for the two circular polarizations or by population differences

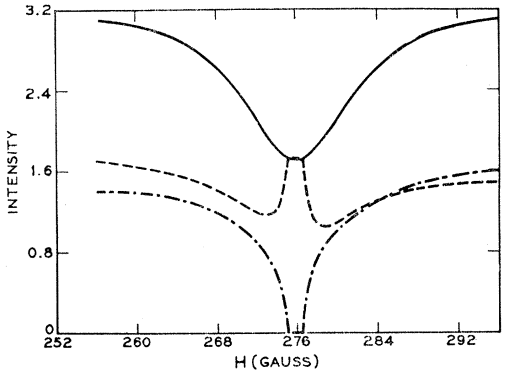

FIG. 18. Mode intensities versus axial magnetic field for 160 MHz detuning, operation on two resonator modes and a 10° field misalignment. Note the absence of the mode intensity crossover. Other parameters are the same as in Fig. 5.

since these discriminate between the competing modes. Q differences for the x-y polarizations cause mode locking which is discussed under Sec. V. The effects of Q differences for the $+-$ polarizations are not easily distinguishable from the effects of nonuniform magnetic sublevel populations since both enter into the theory in the same way. Limiting our discussion of nonuniformities here to the modifications of the intensity curve produced by this kind of asymmetry, we show in Fig. 20 plots of the mode intensities where a small difference has been introduced in the level populations. These differences produce large asymmetries in the tuning curve and cause a shift of the crossover position. In the case shown a population difference of one part in 500 causes a change of 0.66 G in the field at which the mode intensities switch or about one part in five hundred of the Zeeman splitting, thus introducing a potentially serious error in the g-value measurement. The influence of this shift could be reduced by using larger magnetic field values. Since the mode intensity curves are reproduced every time the Zeeman splitting becomes equal to an integral multiple of the mode

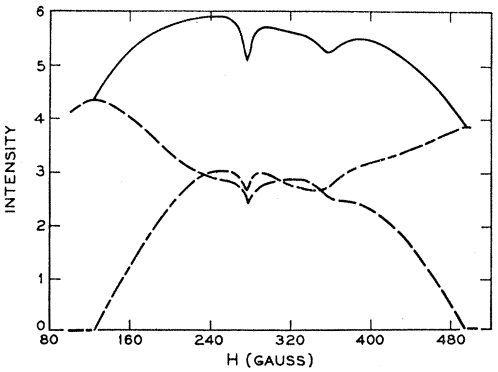

FIG. 19. Mode intensities versus axial magnetic field for 100 MHz detuning and operation on two resonator modes. $J_a=1$, $J_b=1$, $g_a=1.295$, $g_b=0.999$, $\mathfrak{N}=1.20$, $\gamma_a=18.0$ MHz, $\gamma_b=40.0$ MHz, $\gamma_{ab}=120.0$ MHz and $Ku=1010.0$ MHz. Note the separate dips which occur for a Zeeman splitting of the upper state ($H=275.84$ G) and of the lower state ($H=357.53$ G) equal to the resonator mode spacing of 1000 MHz.

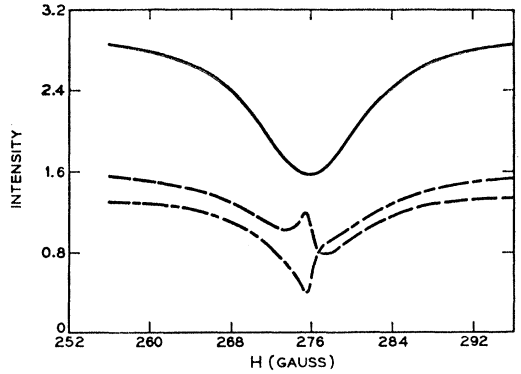

FIG. 20. Mode intensities versus axial magnetic field for the same parameters as Fig. 17, except that a small difference in populations of the sublevels has been introduced by setting $\mathfrak{N}_+$ for the plus polarization equal to 1.201 and $\mathfrak{N}_-$ for the minus polarization equal to 1.199.

spacing the computer analysis predicts, for example, curves identical to those in Fig. 16, with the oscillation on the nth and $(n+20)$th modes of the resonator for a magnetic field swept around 5517 G. In this case the crossover shift would be reduced to 10^{-4} of the Zeeman splitting, rendering the g-value measurement correspondingly more accurate.

To this point we have assumed that the homogeneity of the magnetic field is not a problem. Since magnetic field homogeneities of $1/10^5$ over a 3 cc volume are not difficult to obtain in commerical magnets the field homogeneity would not be the most serious limitation for high-gain lasers. For lower gain and hence longer lasers the field homogeneity, especially for axial field lasers, could prove to be a limiting factor.

By using transverse magnetic fields it would appear possible to keep errors caused by magnetic field inhomogeneities below one part in 10^5, even for lasers of moderate gain and hence longer active region. For example, commercial magnets would provide adequate homogeneity over the approximately 10-cm length required for a laser oscillating on the 6328-Å transition.

For the purpose of discussing g-value measurement we have selected a case where the modes of different polarization oscillate on different resonator modes and only one polarization oscillates on each resonator mode (see Fig. 21). Under these conditions the symmetry of the Zeeman splitting may permit both the $n-1$ and $n+1$ resonator modes to oscillate as well as the nth mode. Hence, to show competition between orthogonally polarized modes oscillating on separate resonator modes in a transverse field one must deal with a three-mode problem. The analysis of this three-mode problem was carried out by a computer program which calculated all possible stationary solutions and then examined each of these solutions for stability as discussed in Sec. IV. In general it was found that only one stable solution exists. The abrupt switch in mode intensities so characteristic of the axial field case did not appear in the transverse field plots run off for similar input parameters. If the losses for the x and y polarizations are identical then the greater gain available to the $\Delta m=0$ transition tends to produce single linear polarization oscillation with the polarization direction parallel to the magnetic field, i.e., along y. However by introducing different losses (e.g., by means of a tilted window) for the two polarizations as indicated in Fig. 21 the y polarization can be suppressed as shown in Fig. 22 or all three modes can be made to oscillate, producing the plot shown in Fig. 23. An unusual feature of the plot in Fig. 23 is the increase in the intensity of the y polarization under central tuning.

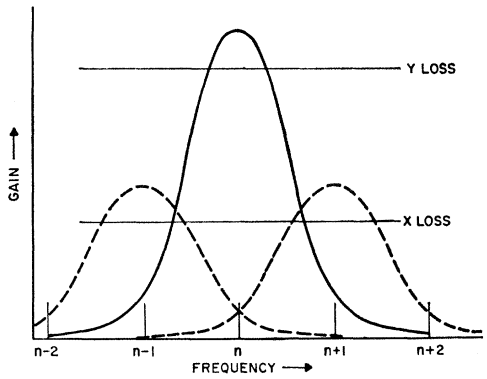

FIG. 21. This figure shows the relative position of the resonator modes and maser gain regions for a transverse magnetic field splitting equal to the mode spacing. It also shows the balance between the gain (x—dashed curves, y—solid curve) and loss (horizontal solid lines) parts of $\alpha_{n\pm 1xx}$ [Eq. (60)] and α_{nyy} [Eq. (61)]. The mode spacing, Zeeman splitting and Doppler widths approximate the values used in the computer plots for Figs. 22 and 23.

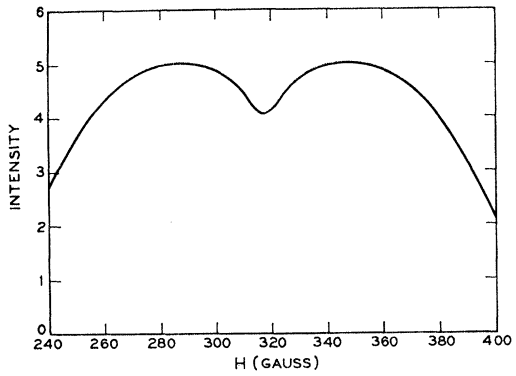

FIG. 22. Mode intensity versus transverse magnetic field for zero detuning. $J_a=1$, $J_b=0$, $g_a=1.3$, $\mathfrak{N}_y=0.02$, $\mathfrak{N}_x=1.15$ (for the resolved $\Delta m=\pm 1$ component) $\gamma_a=30.0$ MHz, $\gamma_b=60.0$ MHz, $\gamma_{ab}=100.0$ MHz, and $Ku=420.0$ MHz. In this case only the x polarization ($\Delta m=\pm 1$) oscillates.

In regard to g-value measurements for the transverse field case, it appears that the intensity crossover between modes of orthogonal polarization will not be generally available. Hence, the dips shown in Figs. 22 and 23 would be the most straightforward means of identifying the field at which the Zeeman splitting equals the mode frequency difference. A crossover in the modes having the x polarization is predicted; however, this crossover would be more difficult to observe in that the modes would have to be interferometrically resolved.

To estimate the accuracy with which a g value could be measured in the absence of a shift of the crossover, we use an experimentally obtained value for the width of the magnetic tuning dip (13.8 G)[12] for the $2s_2-2p_1$ (1.52-μ) transition in neon and a value of the magnetic field (8.23 kG) at which oscillation on other lower gain neon transitions has already been demonstrated.[34] An identification of the dip minimum or intensity crossover to within one-tenth of the linewidth would predict g for the $2s_2$ level to an accuracy of one part in 6000.

The accuracy of these methods appears to be competitive with existing techniques, but considerable care would be required to approach the accuracies of $1/10^5$ and better with which precision double resonance[29] and nuclear-magnetic-resonance measurements are made.

A factor of some use is the dependence of the curve features on J values which permits identification of level J values, even for a case in which the Zeeman splitting is small compared to the Doppler width.[35]

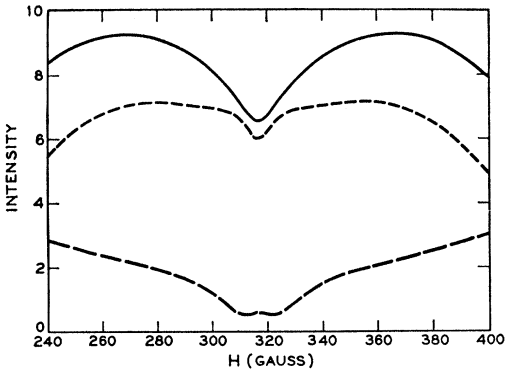

FIG. 23. Same as Fig. 22 except that y loss has been reduced so that $\mathfrak{N}_y=1.44\,\mathfrak{N}_x=1.15$ (for the resolved $\Delta m=\pm1$ components). The plot shows total intensity (solid line), intensity in the x polarization (short dashes), and intensity in the y polarization (long dashes).

In addition the polarized character of the laser radiation can be used to identify the presence of laser action in that the polarization properties, as well as the frequency width and spatial distribution, are distinctly different from those of incoherent radiation.[36] In summary, this theory yields useful information about the presence of laser action, the level J values, and provides a convenient method for measuring lifetimes and g values which may not be easily accessible by other methods.[37]

[34] R. L. Fork and C. K. N. Patel, IEEE Trans. Commun. Electron. **52**, 208 (1964).

[35] W. J. Tomlinson, M. A. Pollack, and R. L. Fork, Appl. Phys. Letters **11**, 150 (1967).

[36] For example, see C. V. Heer, Phys. Rev. Letters **17**, 774 (1966).

[37] Another theoretical treatment has been given by H. R. Schlossberg and A. Javan, Phys. Rev. **150**, 267 (1966). Recent experiments have been performed which support the conclusions given here. See, for example, J. Kannelaud and W. Culshaw, Appl. Phys. Letters **9**, 120 (1966); H. R. Schlossberg and A. Javan, Phys. Rev. Letters **17**, 1242 (1966).